Using entropy balance to determine multiphase flow distribution in thermally decoupled parallel channels with shared inlet and outlet headers

Toochukwu Aka¹, Shankar Narayan^{1,*}

¹Department of Mechanical, Aerospace, and Nuclear Engineering, Rensselaer Polytechnic Institute, 110 8th Street, Troy, NY 12180, USA.

*Corresponding Author: narays5@rpi.edu

ABSTRACT

Multiphase flow with boiling in parallel channels is often an efficient approach to managing heat and energy distribution in several engineering systems. However, two-phase flow with heating in parallel channels is prone to maldistribution, which can result in sub-optimal performance and, in some cases, permanent damage to the system. This challenge requires accurate flow modeling in parallel channels to mitigate or design against the adverse effect of two-phase flow maldistribution. The nonlinear nature of the multiphase flow model can yield multiple solutions for the same operating condition, creating significant challenges in predicting flow distribution. This study addresses this challenge by applying the entropy balance analysis and the conservation of mass, momentum, and energy to predict two-phase flow distribution in two thermally isolated parallel channels with a numerical model. Our model predictions and experiments show that equally distributed flow can become severely maldistributed with a decrease in flow rate, accompanied by a significant (>30%) change in the entropy generation rate. We show that the entropy balance analysis can distinguish between stable and unstable flows and identify the most feasible flow distribution in thermally decoupled parallel channels.

Keywords: Entropy generation, flow distribution, parallel channels, stability, two-phase flow.

1 INTRODUCTION

Flow distribution is critical to multi-channel engineering systems, ranging from heat exchangers and cooling systems to microfluidics and fuel cells. In multi-channel heat exchangers, flow distribution influences the contribution of each channel to heat transfer and the overall heat transfer efficiency [1],[2]. In microfluidics, precise flow distribution is vital for sample manipulation, precise dosing, and efficient reactions [3]. In fuel cells, the distribution of the reactants among parallel flow channels affects electrochemical efficiency and cell lifetime [4]. However, accurately predicting and understanding two-phase flow distribution in parallel channels presents significant challenges.

Several prior studies have been dedicated to analyzing and controlling flow distribution in parallel channels. In our previous study [5], we showed that the thermophysical properties of the channel walls can significantly influence flow maldistribution in two parallel channels. Zhang et al. [6] presented a linear stability analysis to distinguish between stable and unstable flow distributions in a multi-channel evaporator. In Zhang's study, a feedback control strategy was developed to maintain near-equal fluid distribution in a three-parallel channel assembly. Taitel et al. [7] introduced finite disturbances to demonstrate the stability of transient flow distribution solutions. Minzer et al. [8] also performed a linear stability analysis on static flow distribution solutions and showed that flow distribution in a parallel channel assembly depends on the history of the inlet flow rate. Patankar and Salamon [9] employed the thermal resistance model in developing a thermo-fluidic model for a parallel channel heat sink. A linear stability analysis was applied to the unsteady momentum balance equation to distinguish between stable and unstable flow solutions. Jin [10] conducted a numerical analysis of two-phase flow distribution in interconnected parallel

channels. Using coefficients representing degrees of thermal and flow coupling, results from Jin's model indicate that stronger flow and thermal coupling significantly mitigate two-phase flow maldistribution in parallel channels.

We apply the mass, momentum, and energy balance equations to predict the flow distribution in a heated parallel channel system. We also apply linear stability analysis to the unsteady momentum balance equation [6]-[9]. However, in contrast to prior studies that assume channels with homogenous flow, this study considers flow channels with regions consisting of single- and two-phase flows. This study focuses on thermally independent parallel channels, and therefore, unlike the previous models [9], [10], the effect of thermal coupling is absent in the numerical model employed in this study.

Linear stability analysis was commonly applied in previous studies to determine the stability of flow distributions. However, it provides no physical insight into why a stable flow distribution is preferred over other "mathematically feasible" distributions. Also, linear stability analysis cannot differentiate between multiple stable distributions corresponding to a given operating condition. We address these limitations by considering thermodynamic aspects of flow distribution in a parallel channel system.

Entropy balance provides valuable insight into the directionality and inefficiencies of physical processes. Based on the second law of thermodynamics, entropy generation quantifies the rate at which entropy is produced during a physical process. Previous studies have applied entropy analysis in design optimization [11]–[14], flow regime identification [15], and the rederivation of Kirchhoff's law for electric circuits [16]. In this study, we utilize the entropy balance to show the relationship between flow distribution and the entropy production rate in a parallel-channel assembly. We use entropy generation to explain the preference for stable over unstable flow

distributions. Based on the characteristics of entropy generation in the channels and the shared headers of the channel assembly, we show that this approach can determine the most feasible stable states in processes prone to flow maldistribution. Consequently, this approach could aid in accurately modeling multiphase flow in several applications.

2 ANALYSIS

2.1 Physical System

This study focuses on a two-parallel-channel assembly sharing the inlet and exit headers (Figure 1), with dimensions similar to physical systems employed in previous related studies [8],[10],[17]-[23]. Each channel branch has a valve and a long steel tube (30.5 cm) with steady and uniform heating. Each valve has a flow coefficient, K_v (= 10^{-8}), with an orifice opening, A_v ranging from 0 to 100%. Subcooled water (working fluid) enters through the common inlet at T_i (=19 °C) and exits the parallel channel assembly as either liquid, liquid-vapor mixture, or superheated vapor at P_e (= 20 kPa), while heat is transferred from the heaters to the working fluid via the channel walls.

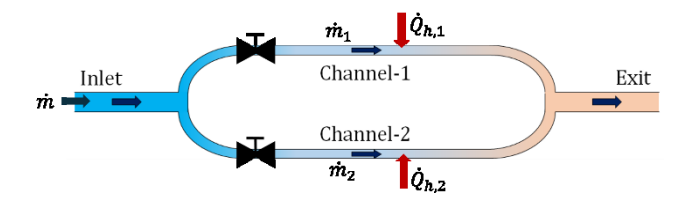


Figure 1. Thermally decoupled parallel channels with a common inlet and exit.

2.2 Governing Equations

The evolution of multiphase flow within a heated channel (Figure 1) can be described using the spatially-lumped form of the unsteady mass conservation (Eq. (1)), momentum balance (Eq. (2)), and energy conservation equations for the fluid and the channel wall (Eqs. (3) and (4)).

$$A_{cs} \left(L \frac{d\rho}{dt} \right)_{ph} = (\dot{m}_i - \dot{m}_e)_{ph} \tag{1}$$

$$\frac{L}{A_{cs}}\frac{d\dot{m}}{dt} = P_i - P_e - \Delta P \tag{2}$$

$$A_{cs} \frac{d(\rho h - P)_{ph}}{dt} = pH_{ph}(T_w - T)_{ph} + \left(\frac{\dot{m}_i h_i - \dot{m}_e h_e}{l}\right)_{ph}$$
(3)

$$\rho_w c_{p,w} \left(V_w \frac{dT_w}{dt} \right)_{ph} = \left(\dot{Q}_h + \dot{m}_i h_i - \dot{m}_e h_e - \dot{Q}_{loss} \right)_{ph} \tag{4}$$

The subscript "ph" denotes a fluid phase region, such as the subcooled liquid, liquid-vapor mixture, and superheated vapor regions in the channel. For example, \dot{m}_{ph} is the mass flow rate in each fluid phase region in the channel, with subscript i denoting inlet and e denoting exit of the region. Similarly, ρ_{ph} , h_{ph} , P_{ph} , T_{ph} , H_{ph} , and l_{ph} are the average fluid density, enthalpy, pressure, temperature, and convective heat transfer coefficient for each phase, respectively. $T_{w,ph}$ and $V_{w,ph}$ describe the average temperature and volume of the channel wall corresponding to each phase. Flow properties related to channel geometry, specifically L, p, and A_{cs} are the channel length, wetted perimeter, and flow cross-sectional area, respectively. Thermophysical properties of the channel wall ρ_w and $c_{p,w}$ are the density and specific heat capacity, respectively.

The pressure drop, ΔP across a channel branch, consists of the valve (ΔP_v) , flow acceleration due to vapor production (ΔP_a) , and frictional (ΔP_f) components, as noted below.

$$\Delta P = \Delta P_v + \Delta P_a + \Delta P_{f,liq} + \Delta P_{f,tp}$$
 (5)

$$\Delta P_v = \frac{1}{\rho_i} \left(\frac{\dot{m}}{K_v A_v} \right)^2 \tag{6}$$

$$\Delta P_a = \dot{m}^2 \left(\frac{1}{\rho_e} - \frac{1}{\rho_i} \right) \tag{7}$$

In this case, A_v is the valve opening, K_v is the valve flow coefficient, ρ_i and ρ_e are the average fluid density at the inlet and exit, respectively. The pressure drop for the liquid phase region $\Delta P_{f,liq}$ is given by the Darcy-Weisbach equation [5] with friction factor obtained from a previous study [24], while the pressure drop in the two-phase region ($\Delta P_{f,tp}$) is computed using the Lockhart and Martinelli correlation [8].

The average heat transfer coefficient for the liquid phase region is given by

$$H_{liq} = \frac{k_{liq} \, Nu_{liq}}{D} \tag{8}$$

where k_{liq} , Nu_{liq} and D are the average fluid thermal conductivity, Nusselt number, and channel internal diameter, respectively. Nu_{liq} is calculated based on the assumption of a uniform heat flux [25]. Similarly, the heat transfer coefficient in the two-phase flow region (H_{tp}) and the critical heat flux (CHF) are computed using correlations from prior studies [26][27]. Apart from the simplification of uniform channel heat flux, we adopt the exit pressure, P_e as the reference pressure for computing saturated fluid properties. Accordingly, the length of the liquid region in a channel, l_{liq} is calculated using inlet, exit, and saturated liquid enthalpies as follows.

$$l_{liq} = \left(\frac{h_{liq,sat}(P_e) - h_i}{h_e - h_i}\right) L \tag{9}$$

The rate of heat loss to the ambient \dot{Q}_{loss} in Eq (4) is unique to a system, which is obtained from experiments as a function of the temperature difference $(T_w - T_\infty)$ and the outer surface area (A), which is discussed later in model validation.

2.2.1 Static Model

The unsteady terms in Eqs. (1) to (4) are eliminated for modeling steady operating conditions, yielding steady forms of mass conservation, momentum balance, and energy conservation equations for an entire channel assuming two-phase flow at the exit.

$$\dot{m}_i = \dot{m}_e = \dot{m} \tag{10}$$

$$P_i - P_e = \Delta P \tag{11}$$

$$p[l_{liq}H_{liq}(T_w - T)_{liq} + l_{tp}H_{tp}(T_w - T)_{tp}] = \dot{m}(h_e - h_i)$$
(12)

$$\dot{m}(h_e - h_i) = \dot{Q}_h - \dot{Q}_{loss} \tag{13}$$

The steady rate of heat transfer into the fluid (\dot{Q}_i) may be expressed as follows.

$$\dot{Q}_i = \dot{m}(h_e - h_i) \tag{14}$$

The average wall temperature (T_w) and fluid temperature (T) for the channel is calculated using the following averaging equations.

$$T_w = \left(T_{liq} + \frac{\dot{Q}_i}{H_{liq}pL}\right)\frac{l_{liq}}{L} + \left(T_{tp} + \frac{\dot{Q}_i}{H_{tp}pL}\right)\frac{l_{tp}}{L} \tag{15}$$

$$T = \frac{T_{liq}l_{liq} + T_{tp}l_{tp}}{L} \tag{16}$$

Eqs. (10) to (13) are solved by posing them as a constrained multivariable function Y(X) and solving it iteratively to find the set of variables X^* that minimizes Y. This minimization problem is expressed as follows,

$$X^* = \arg\min_{F_{min} \le F(X) \le F_{max}} Y(X) \tag{17}$$

where X is a vector of variables updated in each iteration to minimize Y. F(X) is a vector of functions describing the range in which X^* can be found, F_{min} and F_{max} are constraints describing the lower and upper bounds of F(X), respectively. In the context of the current study, for a given

 \dot{m} , \dot{Q}_h and A_v , the steady flow characteristics in a heated channel are obtained by solving the minimization problem with the following parameters and constraints.

$$X = [P_i, \dot{Q}_i] \tag{18}$$

$$Y = \left(\left| \frac{P_i - P_e - \Delta P}{\Delta P} \right| + \left| \frac{\dot{Q}_h - \dot{Q}_i - \dot{Q}_{loss}}{\dot{Q}_{loss}} \right| \right) \tag{19}$$

$$P_i \ge P_e, \ \dot{Q}_i \le \dot{Q}_h, \ Y \le 10^{-4}$$
 (20)

In the case of two parallel channels with heat loads $Q_{h,1}$ and $Q_{h,2}$, valve openings A_{v1} and A_{v2} , and flow rate \dot{m} , the steady flow characteristics are obtained by solving the following minimization problem.

$$X = [P_i, \dot{Q}_{i,1}, \dot{Q}_{i,2}, \dot{m}_1^*]$$
 (21)

$$\dot{m}_2^* = 1 - \dot{m}_1^* \tag{22}$$

$$Y = \frac{1}{\min(\Delta P_1, \Delta P_2)} \sum_{j=1}^{2} \left| P_i - P_e - \Delta P_j \right| + \frac{1}{\min(\dot{Q}_{i,1}, \dot{Q}_{i,2})} \sum_{j=1}^{2} \left| \dot{Q}_{h,j} - \dot{Q}_{i,j} - \dot{Q}_{loss,j} \right|$$
(23)

$$P_i \ge P_e, \ \dot{Q}_{i,1} \le \dot{Q}_{h,1}, \ \dot{Q}_{i,2} \le \dot{Q}_{h,2}, \ \dot{m}_1^* \le 1, \ \lambda \le \lambda_{max}, \ Y \le 10^{-4}$$
 (24)

Here \dot{m}_1^* and \dot{m}_2^* are the flow fractions in the two channels-1 and 2, respectively. λ is a linear stability criterion, which has been used in prior studies [9][28]. λ is the maximum real part of the eigenvalues of the Jacobian matrix of $\frac{d}{dt}\begin{bmatrix} \dot{m}_1^* \\ \dot{m}_2^* \end{bmatrix}$ [28], and λ_{max} is the upper bound for λ . It is generally understood that if $\lambda < 0$, the static solution is stable, and if $\lambda > 0$ the solution is unstable. Therefore, to obtain only stable solutions $\lambda_{max} = 0$.

2.2.2 Transient Model

The unsteady momentum balance equation (Eq. (2)) applied to a two-parallel-channel system allows for predicting the evolution of flow fractions, \dot{m}_1^* and \dot{m}_2^* in a two-channel system.

$$\frac{d}{dt} \begin{bmatrix} \dot{m}_1^* \\ \dot{m}_2^* \end{bmatrix} = \frac{L}{\dot{m}} \begin{bmatrix} \frac{1}{A_{CS,1}} (P_i - P_e - \Delta P_1) \\ \frac{1}{A_{CS,2}} (P_i - P_e - \Delta P_2) \end{bmatrix}$$
(25)

Here $A_{cs,1}$ and $A_{cs,2}$ are the cross-sectional areas of channels-1 and 2, respectively. P_i is obtained from the unsteady momentum balance equation for the whole channel assembly, as shown below.

$$\frac{\dot{m}_{t+\Delta t} - \dot{m}_t}{\Delta t} = \sum_{j=1}^{2} \frac{L}{A_{cs,j}} \left(P_i - P_e - \Delta P_j \right) \tag{26}$$

Here Δt is the time step applied for numerically estimating $d\dot{m}/dt$. Relative to the unsteady mass and energy conservation equations, the unsteady momentum balance equation has the most significant influence on the transient evolution of flow distribution in a two-channel system. Hence, in this study, the transient model solves the main Eqs. (10), (12), (13) and (25).

2.3 Flow Distribution and Entropy Generation

The static solution for different flow rates in a heated channel produces the characteristic 'N' curves (red and black lines), as shown in Figure 2.

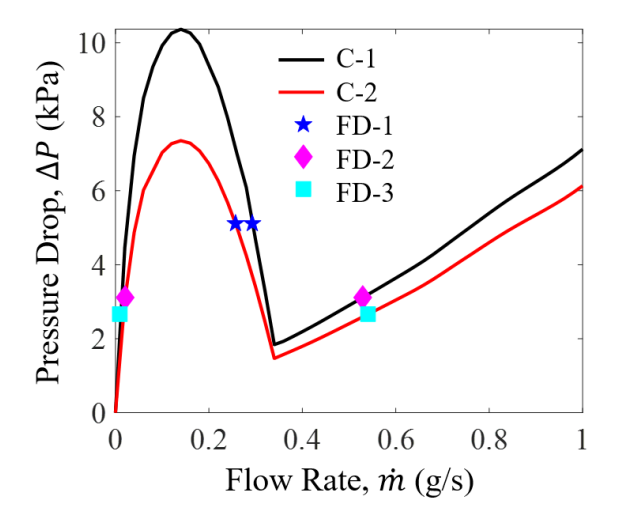


Figure 2. Steady flow distribution solutions in a two-parallel-channel assembly. Lines represent single-channel characteristic pressure curves for channel-1 (C-1) of diameter 1.4 mm and heat load of 60 W, and channel-2 (C-2) of

diameter 1.5 mm and heat load of 60 W. The markers represent different mathematical solutions for flow distributions (FD-1 to 3) corresponding to a total flow rate of $\dot{m} = 0.55$ g/s.

For a given \dot{m} in two parallel channels, the steady flow distributions \dot{m}_1 and \dot{m}_2 each lie on the characteristic curve corresponding to channels-1 and 2 (C-1 and C-2), respectively. From Figure 2, a fixed \dot{m} may yield multiple flow distributions (FD-1, 2, and 3). Linear stability analysis of these solutions [6][8] would indicate that FD-1 and FD-3 are stable and feasible, while FD-2 is unstable, leaving us with two stable, severely maldistributed flow solutions. In this study, we conduct an entropy analysis of each solution to identify the most feasible solution from these "stable" flow distributions.

Entropy analysis is an effective tool for determining the direction of physical processes. For a process to be feasible, the rate of entropy generated (\dot{S}_{gen}) during that process must exceed 0. In a system of N parallel channels, the rate of entropy generation \dot{S}_{gen} at steady state is given by the following equation.

$$\dot{S}_{gen} = \dot{m} \left(s_e(P_e, h_e) - s_i(P_i, T_i) \right) - \sum_{j=1}^{N} \frac{\dot{Q}_{i,j}}{T_{w,j}}$$
(27)

The specific entropies at the inlet (s_i) and outlet (s_e) of the channel assembly are functions of inlet pressure P_i and temperature T_i , and exit pressure P_e and specific enthalpy h_e , respectively. Entropy generated within a heated parallel channel assembly consists of entropy generated within each channel flow stream, entropy generated from splitting the flow at the shared inlet, and entropy generated from mixing the flow at the shared exit of the network. Entropy generated at the inlet is typically negligible relative to other contributions [18]. Hence, in this simple arrangement, \dot{S}_{gen} can be expressed using the following equation.

$$\dot{S}_{gen} = \dot{S}_{gen,mix} + \sum_{j=1}^{N} \dot{S}_{gen,j}$$
 (28)

Here $\dot{S}_{gen,j}$ is the entropy generation rate within each channel of the parallel network. $\dot{S}_{gen,mix}$ is the rate of entropy generated by heat transfer and expansion corresponding to fluid emerging from each channel and mixing. For an adiabatic mixing process involving multiple streams with no heat loss to the environment, $\dot{S}_{gen,mix}$ is a function of the flow distribution $\dot{m}_j^* = \frac{\dot{m}_j}{\dot{m}}$ and the heat load distribution $\dot{Q}_{h,j}^* = \frac{\dot{Q}_{h,j}}{\dot{Q}_h}$.

$$\dot{S}_{gen,mix} = \dot{m} \left(s_{mix} - \sum_{j=1}^{N} \dot{m}_{j}^{*} s_{e,j} (P_{e}, h_{e,j}) \right)$$
(29)

$$h_{e,j} = h_i + \frac{\dot{Q}_{h,j}^* \dot{Q}_h}{\dot{m}_i^* \dot{m}} \tag{30}$$

3 MODEL VALIDATION

3.1 Testbed Description

An experimental testbed consisting of a heated tank, gear pump, electronic valve, and evaporator assembly was constructed (Figure 3) to validate the static and dynamic models. The evaporator assembly consists of two capillary steel tubes with an internal diameter of 1.4 mm, outer diameter of 3.18 mm, and length of 30.5 cm, wrapped with 125 W-rated rope heaters and an outer layer of fiberglass insulation. Coupled to the ends of each steel tube are stop valves and flow meters (Omega FLR-1008ST, ± 0.03 g/s). Four thermocouples (Omega T-type, $\pm 1^{\circ}$ C) are attached to the wall of each tube at equidistant locations to monitor the wall temperature. Pressure sensors (Omega PX309-030A5V, ± 0.52 kPa) and additional thermocouples are positioned at the inlet and exit of the assembly to monitor flow properties at these locations.

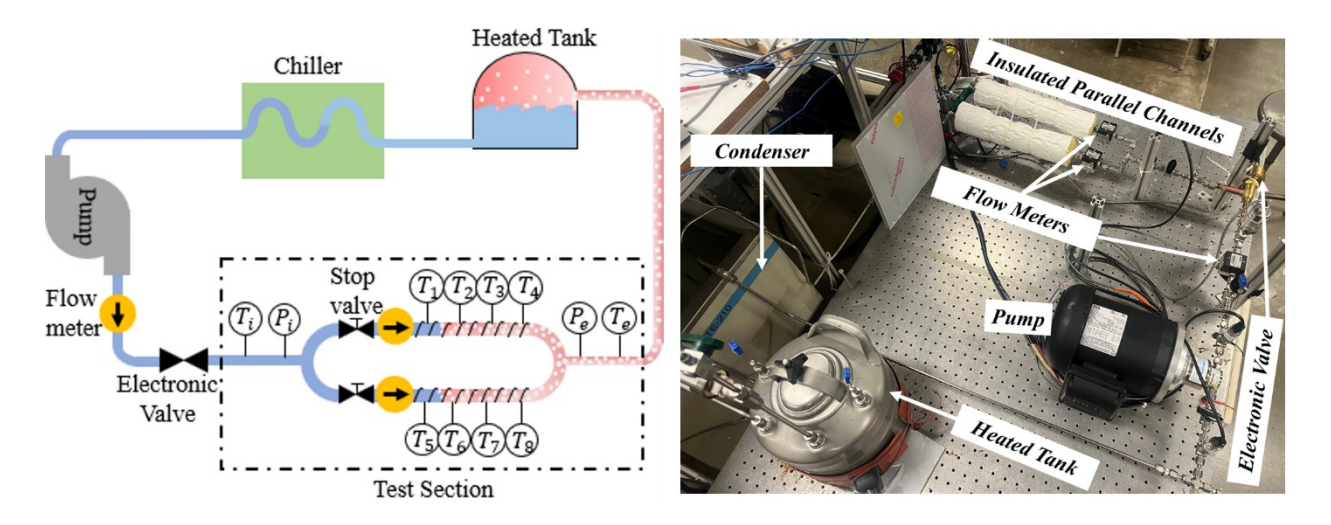


Figure 3. The experimental testbed to study static and dynamic characteristics of flow maldistribution.

Heat loss characterization for different mass flow rates is shown in Figure 4. For these experiments conducted in a controlled lab environment, heat loss takes place to the ambient air at the temperature T_{∞} (= 24 °C). The heat loss from the channel to the environment, expressed in non-dimensional form in terms of Nusselt number, is $Nu_{loss} = 9.7 \pm 0.5$. The range of flow rates tested in the experiment corresponds to $270 \pm 23 \le Re_D \le 855 \pm 30$.

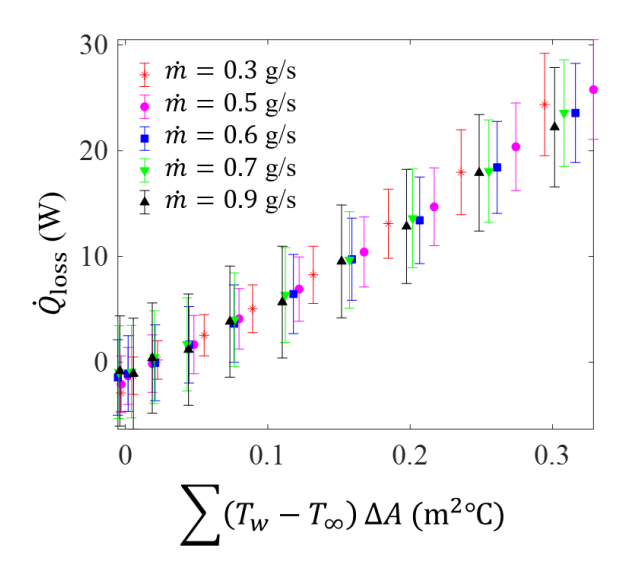


Figure 4. Heat loss characterization.

3.2 Model Validation

In Figure 5(a), a heat load of 70 W is supplied to each channel while fluid is supplied through the inlet header to the parallel channel assembly. Initially, at a high flow rate, the flow is uniformly distributed among each channel (Figure 5(a-i)) while \dot{S}_{gen} decreases with \dot{m} (Figure 5(a-ii)). However, as \dot{m} is gradually decreased, the flow becomes severely maldistributed and \dot{S}_{gen} increases. After the flow distribution becomes nonuniform, \dot{S}_{gen} decreases with a subsequent decrease in \dot{m} . The maximum uncertainties in flow fraction (\dot{m}^*) and entropy generation rate (\dot{S}_{gen}) are ± 0.15 and 0.0025 W/K, respectively [29].

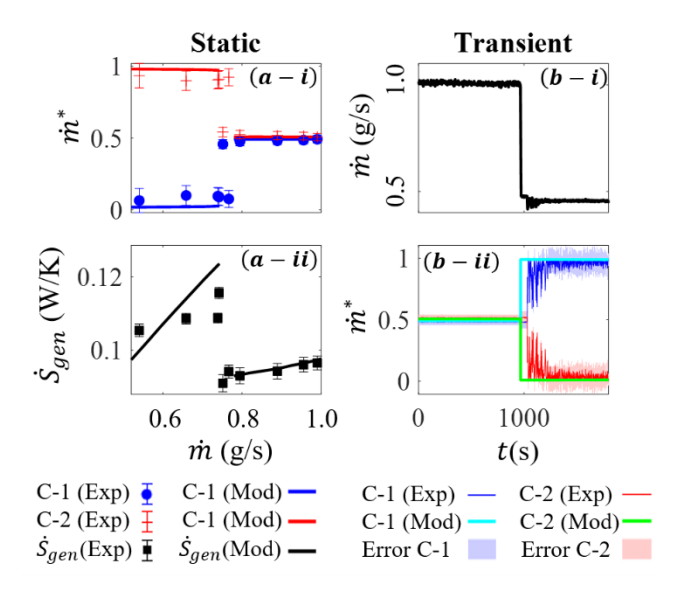


Figure 5. Model validation for both static and dynamic conditions.

For the transient experiment, channel-1 and channel-2 are supplied with a steady heat load of 40 W and 60 W, respectively, while the assembly is initially supplied with a flow rate \dot{m} of 1 g/s, as shown in Figure 5(b-i). Like the static experiment, initially, the flow is equally distributed in the two channels. However, when the \dot{m} is abruptly decreased to 0.46 g/s, the flow becomes severely maldistributed, with channel-1, in this case, receiving the bulk of the flow and channel-2 experiencing almost no flow, as shown in Figure 5(b-ii). For the transient experiment, the

maximum uncertainty in the flow fraction (\dot{m}^*) is ± 0.11 [29]. The static and transient model predictions agree with experimental data.

In the subsequent application of the model for predicting flow distribution at different conditions, the channels are assumed to be perfectly insulated ($\dot{Q}_{loss}=0$). For most cases, the model considers a mass flow rate, \dot{m} in the range $0 < \dot{m} < 1.2$ g/s and channel diameters, D such that 1.1 < D < 1.7 mm. The flow conditions analyzed in this study correspond to $0 < Re_D < 1125$.

4 RESULTS

4.1 Entropy Generation in a Single-Channel

Flow boiling in a single channel is characterized by thermal and hydraulic resistances. These resistances are sources of irreversibility and contribute significantly to entropy production within the channel. Hydraulic resistance, primarily due to frictional forces, causes a pressure drop $\Delta P = P_i - P_e$ as flow occurs through the channel. Likewise, heat transfer across a finite thermal resistance requires a temperature difference, $\Delta T_w = T_w - T_f$ between the wall and the fluid. Hence, ΔP and ΔT_w represent the departure from ideal flow and heat transfer with no entropy generation. Therefore, ΔP and ΔT_w are indirect measures of irreversibility in flow and heat transfer processes, respectively. Figure 6 shows the variation of ΔP , ΔT_w , and \dot{S}_{gen} with \dot{m} for different combinations of heat loads (\dot{Q}_h) and channel internal diameter (D) for a single channel.

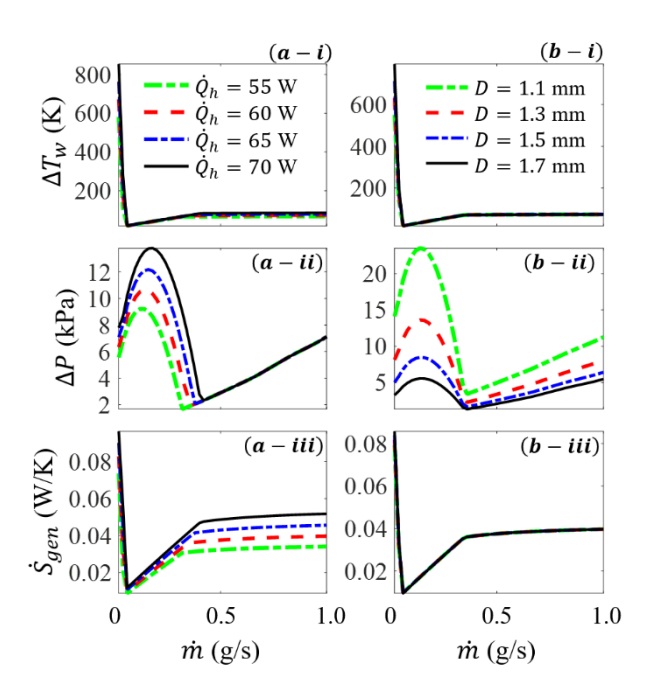


Figure 6. Variation of single-channel steady-state flow properties with (a) varying \dot{m} and \dot{Q}_h at D=1.4 mm, and (b) varying \dot{m} and D at $\dot{Q}_h=60$ W.

A large \dot{m} generally corresponds to single-phase liquid at the channel exit, indicated by a positive slope of curves on the far right of each plot. As \dot{m} decreases, the fluid at the channel exit becomes a two-phase vapor-liquid mixture, resulting in a change in slope from positive to negative in the ΔP versus \dot{m} curves. The slope of the curves for other parameters remains positive but becomes steeper, indicating rapid variation with changes in \dot{m} . A very small \dot{m} on the far left of each plot corresponds to superheated vapor flow at the channel exit. In this region, the slope of the ΔP versus \dot{m} curves becomes positive again, while the other curves change from positive to a steep negative slope due to the occurrence of critical heat flux (CHF) – a region corresponding to significantly inefficient heat transfer or high ΔT_w , and consequently, large irreversibility (\dot{S}_{gen}).

The variation in \dot{Q}_h has no significant impact on ΔP for single-phase liquid at the channel exit, as shown in Figure 6(a-ii). However, ΔP increases with an increase in \dot{Q}_h when two-phase mixtures and superheated vapor exit the channels. A change in D results in a significant variation in ΔP ,

with ΔP increasing for smaller D in Figure 6(b-ii) due to a larger hydraulic resistance to flow. A larger \dot{Q}_h increases ΔT_w and \dot{S}_{gen} (Figure 6(a-i) and Figure 6(a-iii)), while variations in D have no significant impact on ΔT_w and \dot{S}_{gen} (Figure 6(b-i) and Figure 6(b-iii)). Generally, both flow and heat transfer irreversibilities contribute to entropy production to different extents. For the system analyzed in this study, thermal irreversibilities are more significant than flow irreversibilities. Consequently, for a fixed flow rate, \dot{m} and heat load, \dot{Q}_h although a smaller diameter, D corresponds to larger viscous losses, the corresponding increase in \dot{S}_{gen} is not significant, as evident in Figure 6(b-ii). On the other hand, an increase in \dot{Q}_h , keeping \dot{m} and D fixed corresponds to higher ΔT_w and thermal irreversibilities with a noticeable rise in \dot{S}_{gen} . The variation in ΔT_w and \dot{S}_{gen} versus \dot{m} are similar. These curves differ from the trends in ΔP versus \dot{m} , which also indicate that the dominant contribution towards irreversibility (in this case) is associated with heat transfer rather than flow characteristics.

4.2 Entropy Generation due to Adiabatic Mixing of Fluid

The fraction of flow and heat load in each channel influences $\dot{S}_{gen,mix}$. Figure 7 describes the variation of $\dot{S}_{gen,mix}$ with the variation in the fraction $\dot{m}_j^* = \frac{\dot{m}_j}{\dot{m}}$ of the total flow rate \dot{m} , and fraction $\dot{Q}_{h,j}^* = \frac{\dot{Q}_{h,j}}{\dot{Q}_h}$ of the total heat load \dot{Q}_h on channel j of a parallel assembly with two channels. Therefore, for uniformly distributed flow and heating power, $\dot{m}_j^* = \dot{Q}_{h,j}^* = 0.5$.

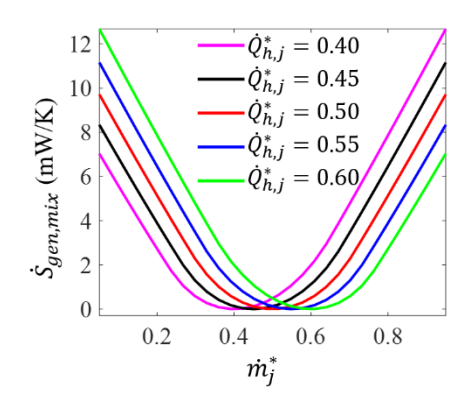


Figure 7. Variation of $\dot{S}_{gen,mix}$ with \dot{m}_j^* and $\dot{Q}_{h,j}^*$ for $\dot{m}=1$ g/s and $\dot{Q}_h=100$ W.

The $\dot{S}_{gen,mix}$ versus m_j^* corresponding to a $\dot{Q}_{h,j}^*$ is typically a nonlinear curve with a minimum at $\dot{m}_j^* = \dot{Q}_{h,j}^*$. At this point, the thermal energy content of both fluid streams is the same, and hence, there is no entropy generation due to the irreversible fluid-to-fluid heat transfer during the mixing process. At points where $\dot{m}_j^* < \dot{Q}_{h,j}^*$, $\dot{S}_{gen,mix}$ increases with an increase in $\dot{Q}_{h,j}^*$, and at points where $\dot{m}_j^* > \dot{Q}_{h,j}^*$, $\dot{S}_{gen,mix}$ increases with a decrease in $\dot{Q}_{h,j}^*$. This variation shows that the maximum $\dot{S}_{gen,mix}$ occurs when the flow is highly maldistributed (far right or far left regions of the plot), corresponding to large heat loads with low flow rates and low heat loads with high flow rates.

4.3 Entropy Generation in a Two-channel Assembly

Figure 8 describes the variation in ΔP , $\Delta T_{w,1}$, $\Delta T_{w,2}$, \dot{m}_1^* , \dot{m}_2^* , and \dot{S}_{gen} with \dot{m} , the combined flow rate in the two-channel assembly. For large values of \dot{m} , the flow is almost uniformly distributed among the channels, $\Delta T_{w,1}$ and $\Delta T_{w,2}$ are similar and constant. As \dot{m} decreases, ΔP and \dot{S}_{gen} decrease as well.

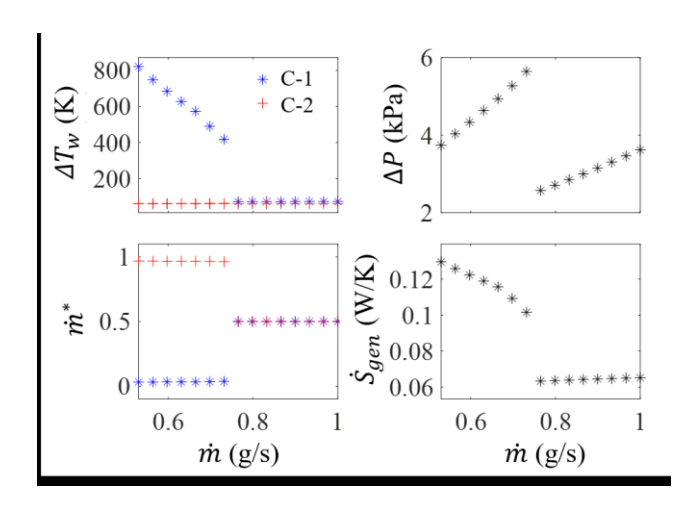


Figure 8. Effect of flow maldistribution on flow properties of a two parallel channel assembly with channel-1 (C-1) characteristics corresponding to $D_1=1.4$ mm, $\dot{Q}_{h,1}=60$ W, and $A_{v1}=100$ % and channel-2 (C-2) characteristics corresponding to $D_2=1.4$ mm, $\dot{Q}_{h,2}=60$ W, and $A_{v2}=50$ %.

With a further decrease in \dot{m} , phase change in the working fluid triggers severe flow maldistribution, characterized by increased flow in channel-2 (C-2) and decreased flow in channel-1 (C-1). This results in a sharp increase in $\Delta T_{w,1}$ and ΔP across the assembly but no significant change in $\Delta T_{w,2}$. The onset of CHF in channel-1 and increased hydraulic resistance in channel-2 causes \dot{S}_{gen} to increase suddenly with the onset of flow maldistribution. After the onset of flow maldistribution, the rising $\Delta T_{w,1}$ due to lower \dot{m} causes a further increase in \dot{S}_{gen} . The influence of environmental heat loss, \dot{Q}_{loss} on \dot{S}_{gen} can be seen in the significant difference in the slopes of \dot{S}_{gen} versus \dot{m} in Figure 8 ($\dot{Q}_{loss} = 0$) and Figure 5 ($\dot{Q}_{loss} > 0$) in the maldistributed flow region.

4.4 Entropy Generation and Stability of a Flow Distribution

Typically, the predicted solutions for multiphase flow distribution in parallel channels are not unique (e.g., Figure 2). Modeling could predict both stable and unstable flow distributions for the same operating conditions. To address this aspect, as mentioned earlier, a stability criterion λ derived from the linear perturbation theory is often used to distinguish between stable ($\lambda < 0$)

and unstable ($\lambda > 0$) flow distributions, as shown in Figures 9(a-i) and 9(b-i). To provide a thermodynamic perspective on the stability of flow distributions, Figure 9 compares the \dot{S}_{gen} for stable flow distribution (black) with an unstable flow distribution profile (red).

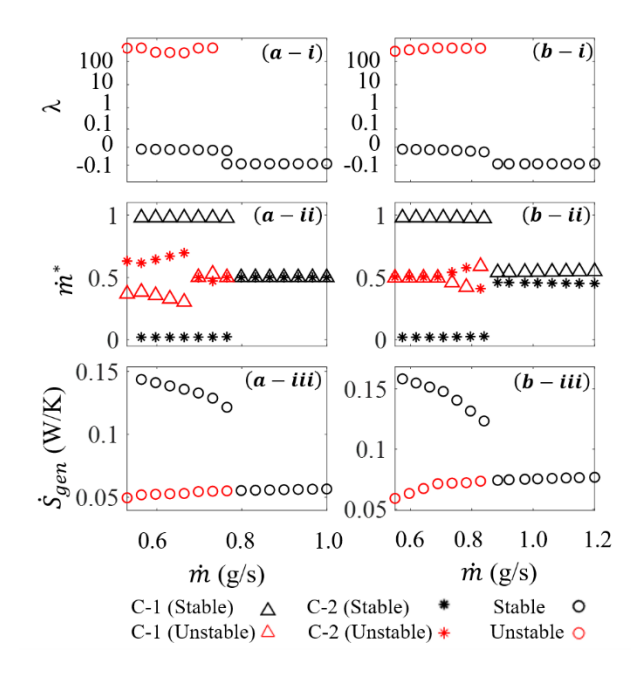


Figure 9. Comparison between stable ($\lambda < 0$) and unstable ($\lambda > 0$) flow distribution profiles for (a) $D_1 = D_2 = 1.4$ mm, $A_{v1} = A_{v2} = 100\%$, and $\dot{Q}_{h,1} = 50$ W and $\dot{Q}_{h,2} = 70$ W, and (b) $D_1 = D_2 = 1.4$ mm, $\dot{Q}_{h,1} = \dot{Q}_{h,2} = 60$ W, $A_{v1} = 100\%$ and $A_{v2} = 50\%$.

For the results in Figure 9(a), the channels have identical tube geometries and upstream valve openings, with different heat loads of $\dot{Q}_{h,1} = 50 \text{ W}$, and $\dot{Q}_{h,2} = 70 \text{ W}$. For a large \dot{m} , flow is uniformly distributed and stable, while for small \dot{m} , the predicted flow distributions can be either severely maldistributed and stable or moderately nonuniform and unstable, as shown in Figures 9(a-i) and 9(a-ii). For the results in Figure 9(b), the channels have identical geometries and heat loads, with different valve openings at $A_{v1} = 100\%$ and $A_{v2} = 50\%$. Here, for large \dot{m} , the flow solutions are stable but expectedly unequally distributed due to the different valve settings. However, for a small \dot{m} , the model-predicted flow distribution can be either severely

maldistributed and stable or uniform and unstable, as shown in Figures 9(b-i) and 9(b-ii). In both cases involving slightly different operating conditions for the two parallel channels, Figures 9(a-iii) and 9(b-iii) show that the \dot{S}_{gen} associated with the stable maldistributed flow solutions is greater than the \dot{S}_{gen} associated with the unstable flow predictions. This observation indicates that the maldistributed flow is thermodynamically preferred over other model-predicted flow distributions that satisfy the conservation laws and system constraints. Such severe maldistributions have been observed to occur in experiments, as shown in Figure 5.

4.5 Entropy Generation and Severely Maldistributed Flow Solutions

Based on linear stability criteria shown in Figure 9, severely maldistributed flow solutions are inherently stable but could be non-unique (Figure 2), which limits the application of the linear stability analysis since it only distinguishes between stable and unstable flow distributions. For a given operating condition in a parallel channel system consisting of two perfectly identical tubes, the severely maldistributed flow solutions are mirror images of each other with the flow magnitudes reversed. These solutions are also indistinguishable when considering extensive thermodynamic properties (like \dot{S}_{gen}) associated with each solution. However, with the introduction of non-uniformities in the individual channels, as expected in practical applications, the entropy balance analysis can evaluate the feasibility of each solution to determine the expected final state during flow maldistribution.

Let us now consider a flow condition with severe maldistribution in a perfectly insulated $(\dot{Q}_{loss} = 0 \rightarrow \dot{Q}_i = \dot{Q}_h)$ two-channel system with the following steady flow settings: flow rate \dot{m} , identical heat loads $(\dot{Q}_{h,1} = \dot{Q}_{h,2} = \dot{Q}_h/2)$, and identical internal diameters $(D_1 = D_2)$. For these

settings, the predicted flow maldistributions, $\dot{m}_1 \ll \dot{m}_2$ and $\dot{m}_1 \gg \dot{m}_2$, are equivalent with respect to the entropy generation, $\dot{S}_{gen,0}$. From Eq. (28),

$$\dot{S}_{gen,0} = \dot{S}_{gen,1} + \dot{S}_{gen,2} + \dot{S}_{gen,mix} \tag{31}$$

where $\dot{S}_{gen,1}$ and $\dot{S}_{gen,2}$ are the rate of entropy generation in channels-1 and 2, respectively, and $\dot{S}_{gen,mix}$ corresponds to entropy generation due to the mixing of the two fluid streams.

Introducing non-uniformities in the channel heat loads and dimensions while maintaining the same total flow rate and total heat load will result in a change in the entropy generation rate by $d\dot{S}_{gen,0}$. The rate of entropy generation \dot{S}_{gen} is then given by

$$\dot{S}_{gen} = \dot{S}_{gen,0} + d\dot{S}_{gen,0} \tag{32}$$

where $d\dot{S}_{gen,0}$ can be expressed using the chain rule as follows.

$$d\dot{S}_{gen,0} = \sum_{j=1}^{2} \left(\frac{\partial \dot{S}_{gen,j}}{\partial \dot{m}_{j}} d\dot{m}_{j} + \frac{\partial \dot{S}_{gen,j}}{\partial \dot{Q}_{h,j}} d\dot{Q}_{h,j} + \frac{\partial \dot{S}_{gen,j}}{\partial D_{j}} dD_{j} + \frac{\partial \dot{S}_{gen,mix}}{\partial \dot{Q}_{h,j}^{*}} d\dot{Q}_{h,j}^{*} + \frac{\partial \dot{S}_{gen,mix}}{\partial \dot{m}_{j}^{*}} d\dot{m}_{j}^{*} \right) (33)$$

The constant total mass flow and heat loads in the two channels would require the following.

$$d\dot{m}_1 = -d\dot{m}_2 \tag{34}$$

$$d\dot{Q}_{h,1} = -d\dot{Q}_{h,2} \tag{35}$$

From the momentum balance equation, \dot{m}_j is a function of $\dot{Q}_{h,j}$, D_j , and the pressure drop ΔP , as shown in Figures 6(a-ii) and 6(b-ii). Hence, $d\dot{m}_i$ can be expressed using the chain rule as:

$$d\dot{m}_{j} = \frac{\partial \dot{m}_{j}}{\partial \Delta P} d\Delta P + \frac{\partial \dot{m}_{j}}{\partial \dot{Q}_{h,j}} d\dot{Q}_{h,j} + \frac{\partial \dot{m}_{j}}{\partial D_{j}} dD_{j}$$
(36)

Based on the trends shown in Figures 6 and 7, the characteristics of the partial derivative terms in Eqs. (33) and (36) for a severely maldistributed flow in the two parallel channels are summarized

in Table 1. The magnitudes of the partial derivatives are later used to predict the entropy generation rate and the expected flow distribution in the parallel channels.

Table 1. Effect of system parameters on $\dot{S}_{gen,j}$ and \dot{m}_j

	Reference Figures	$\dot{m}_j \approx \dot{m}$	$\dot{m}_j \approx 0$
$rac{\partial \dot{S}_{gen,j}}{\partial \dot{m}_{j}}$	6(a-iii) or 6(b-iii)	> 0	≪ 0
$\frac{\partial \dot{S}_{gen,j}}{\partial \dot{Q}_{h,j}}$	6(a-iii)	> 0	> 0
$\frac{\partial \dot{S}_{gen,j}}{\partial D_j}$	6(b-iii)	≈ 0	≈ 0
$\frac{\partial \dot{S}_{gen,mix}}{\partial \dot{Q}_{h,j}^*}$	7	< 0	> 0
$rac{\partial \dot{\mathcal{S}}_{gen,mix}}{\partial \dot{m}_{j}^{*}}$	7	> 0	< 0
$rac{\partial \dot{m}_j}{\partial \Delta P}$	6(a-ii) or 6(b-ii)	> 0	> 0
$rac{\partial \dot{m}_j}{\partial \dot{Q}_{h,j}}$	6(a-i)	≈ 0	< 0
$\frac{\partial \dot{m}_j}{\partial D_j}$	6(b-i)	> 0	> 0

4.5.1 Variation in Diameter

By introducing a minor non-uniformity in the channel geometry by varying one of the diameters, Eq. (33) reduces to the following.

$$d\dot{S}_{gen,0} = \sum_{j=1}^{2} \left(\frac{\partial \dot{S}_{gen,j}}{\partial \dot{m}_{j}} d\dot{m}_{j} + \frac{\partial \dot{S}_{gen,j}}{\partial D_{j}} dD_{j} + \frac{\partial \dot{S}_{gen,mix}}{\partial \dot{m}_{j}^{*}} d\dot{m}_{j}^{*} \right)$$
(37)

Eqs. (34) and (36) give the following equation for the two channels.

$$\frac{\partial \dot{m}_1}{\partial \Delta P} d\Delta P + \frac{\partial \dot{m}_1}{\partial D_1} dD_1 = -\left(\frac{\partial \dot{m}_2}{\partial \Delta P} d\Delta P + \frac{\partial \dot{m}_2}{\partial D_2} dD_2\right) \tag{38}$$

If D_1 is increased by an infinitesimal amount dD ($dD_1 > 0$) without changing D_2 ($dD_2 = 0$), and the maldistributed flow is such that $\dot{m}_1 \approx \dot{m}$ and $\dot{m}_2 \approx 0$, then from Table 1, Eq. (38) is satisfied only if $d\Delta P < 0$, which implies $d\dot{m}_2 < 0$ and $d\dot{m}_2^* < 0$ (from Eq. (36)), and consequently, $d\dot{m}_1 > 0$ and $d\dot{m}_1^* > 0$ (Eq. (34)). Based on the magnitude of the partial derivatives in Table 1 for channels-1 and 2, we deduce that all the terms in Eq. (37) are ≥ 0 for this case, implying $d\dot{S}_{gen,0} > 0$. Hence, with D_1 only slightly larger than D_2 and all other conditions being uniform across channels-1 and 2, a maldistributed flow with $\dot{m}_1 \approx \dot{m}$ and $\dot{m}_2 \approx 0$ is favored since it increases the irreversibility of the system ($d\dot{S}_{gen,0} > 0$).

Alternately, if D_2 is decreased by dD ($dD_2 < 0$) without changing D_1 ($dD_1 = 0$), and the maldistributed flow is such that $\dot{m}_1 \approx 0$ and $\dot{m}_2 \approx \dot{m}$, then from Table 1, Eq. (38) is satisfied if $d\Delta P > 0$, which implies $d\dot{m}_1 > 0$ and $d\dot{m}_1^* > 0$ (from Eq. (36)), and consequently $d\dot{m}_2 < 0$ and $d\dot{m}_2^* < 0$ (Eq. (34)). Again, based on the magnitude of the partial derivatives in Table 1, we expect all the terms in Eq. (37) to be ≤ 0 , implying $d\dot{S}_{gen,0} < 0$. Hence, for these conditions wherein D_1 is only slightly larger than D_2 with all other operational parameters being uniform across the channels, a maldistributed flow such that $\dot{m}_1 \approx 0$ and $\dot{m}_2 \approx \dot{m}$ is unlikely.

Also, in this case, if D_1 and D_2 differ only by an infinitesimal amount dD, an equally distributed two-phase flow $(\dot{m}_1 \approx \dot{m}_2 \approx \dot{m}/2)$ is unlikely. We know this from the previous section (4.5) since the corresponding \dot{S}_{gen} is much less than the \dot{S}_{gen} for a severely maldistributed flow, which is thermodynamically preferred. Even the stability criterion (λ) derived from the linear perturbation theory would indicate a maldistributed flow. Therefore, for the boiling-induced two-phase flow in the parallel channels, where $\dot{Q}_{h,1} = \dot{Q}_{h,2}$ and D_1 is only slightly larger than D_2 , \dot{S}_{gen} corresponding to $\dot{m}_1 \gg \dot{m}_2$ is greater than \dot{S}_{gen} corresponding to $\dot{m}_1 \ll \dot{m}_2$. Based on the magnitude of \dot{S}_{gen} ,

 $\dot{m}_1 \gg \dot{m}_2$ is thermodynamically more favorable and is likely the final maldistributed state. This result implies that when flow maldistribution occurs during boiling-induced two-phase flow in a two-parallel-channel assembly with slightly differing internal diameters and equal heat loads, the flow is highly concentrated in the channel with the larger diameter while that with the smaller diameter is starved of fluid. This outcome is corroborated in previous experimental studies [5],[30].

4.5.2 Variations in Heat Load

If non-uniformity is introduced by adding $d\dot{Q}_h$ to channel-1 and decreasing $d\dot{Q}_h$ from channel-2, we have $d\dot{Q}_{h,1} > 0$ and $d\dot{Q}_{h,1}^* > 0$, while $d\dot{Q}_{h,2} < 0$ and $d\dot{Q}_{h,2}^* < 0$. Eq. (33) reduces to the following.

$$d\dot{S}_{gen,0} = \sum_{j=1}^{2} \left(\frac{\partial \dot{S}_{gen,j}}{\partial \dot{m}_{j}} d\dot{m}_{j} + \frac{\partial \dot{S}_{gen,j}}{\partial \dot{Q}_{h,j}} d\dot{Q}_{h,j} + \frac{\partial \dot{S}_{gen,mix}}{\partial \dot{Q}_{h,j}^{*}} d\dot{Q}_{h,j}^{*} + \frac{\partial \dot{S}_{gen,mix}}{\partial \dot{m}_{j}^{*}} d\dot{m}_{j}^{*} \right)$$
(39)

In this case, Eqs. (34) and (36) yield the following.

$$\frac{\partial \dot{m}_{1}}{\partial \Delta P} d\Delta P + \frac{\partial \dot{m}_{1}}{\partial \dot{Q}_{h,1}} d\dot{Q}_{h,1} = -\left(\frac{\partial \dot{m}_{2}}{\partial \Delta P} d\Delta P + \frac{\partial \dot{m}_{2}}{\partial \dot{Q}_{h,2}} d\dot{Q}_{h,2}\right) \tag{40}$$

If the maldistributed flow is such that $\dot{m}_1 \approx 0$ and $\dot{m}_2 \approx \dot{m}$, then from Table 1, Eq. (40) is satisfied if $d\Delta P > 0$, which implies $d\dot{m}_2 > 0$ and $d\dot{m}_2^* > 0$ (using Eq. (36)), and consequently, $d\dot{m}_1 < 0$ and $d\dot{m}_1^* < 0$. Based on Table 1, for j=1 and 2, we can deduce that all the terms in Eq. (39) are 0 = 0, except $\frac{\partial \dot{s}_{gen,2}}{\partial \dot{q}_{h,2}} d\dot{q}_{h,2}$, which is 0 = 0. However, from Table 1, $\left| \frac{\partial \dot{s}_{gen,1}}{\partial \dot{m}_1} \right| \gg \left| \frac{\partial \dot{s}_{gen,2}}{\partial \dot{q}_{h,2}} \right|$, implying $d\dot{s}_{gen,0} > 0$. In essence, for two channels that are geometrically identical and differ only slightly in the wall heat loads such that $\dot{q}_{h,1}$ is marginally larger than $\dot{q}_{h,2}$, the maldistributed flow with $\dot{m}_1 \approx 0$ and $\dot{m}_2 \approx \dot{m}$ is favored since it tends to increase the system's irreversibility.

Alternately, if the maldistributed flow is such that $\dot{m}_1 \approx \dot{m}$ and $\dot{m}_2 \approx 0$, we can go through a similar reasoning to conclude that $d\dot{m}_1 > 0$ and $d\dot{m}_1^* > 0$, and consequently, $d\dot{m}_2 < 0$ and $d\dot{m}_2^* < 0$. More importantly, for these conditions, $d\dot{S}_{gen,0} < 0$.

Therefore, for a case of a severely maldistributed flow in a two parallel channel system with $D_1 = D_2$ and $\dot{Q}_{h,1}$ only slightly larger than $\dot{Q}_{h,2}$, the \dot{S}_{gen} corresponding to $\dot{m}_1 \ll \dot{m}_2$ is greater than the \dot{S}_{gen} corresponding to $\dot{m}_1 \gg \dot{m}_2$. Even in this case, equally distributed flow $(\dot{m}_1 \approx \dot{m}_2 \approx \dot{m}/2)$ corresponds to \dot{S}_{gen} much less than that of a maldistributed flow. Therefore, based on the magnitude of \dot{S}_{gen} for these operating conditions, $\dot{m}_1 \ll \dot{m}_2$ is thermodynamically favored and is likely the final maldistributed state. Hence, when flow maldistribution occurs in a two parallel channel assembly with slightly varying heat loads and identical geometry, flow is concentrated in the channel with a smaller heat load while the other channel with a larger heat load is starved of the fluid. This outcome is also corroborated in previous studies [5],[30].

Based on the conclusions from both scenarios, Figure 10 compares the \dot{S}_{gen} for maldistributed flow states (black) that are likely to occur with the \dot{S}_{gen} for unlikely maldistributed flow states (red). All operational conditions are identical except for the channel internal diameters in Figure 10(a) and channel heat loads in Figure 10(b). At higher total flow rates, the flow distribution is uniform in the two channels (Figures 10(a-i) and 10(b-i)). The model predictions do not indicate any deviations in \dot{S}_{gen} (Figures 10(a-ii) and 10(b-ii)). However, at lower flow rates, flow maldistribution is expected. The expected flow distribution is a small flow rate in channel-1 and a large flow rate in channel-2 since $D_1 < D_2$ and $\dot{Q}_{h,1} > \dot{Q}_{h,2}$. The unlikely flow distribution is a large flow fraction in channel-1 and a smaller flow fraction in channel-2. A comparison of \dot{S}_{gen} associated with both flow solutions ($\dot{m}_1 \gg \dot{m}_2$ and $\dot{m}_1 \ll \dot{m}_2$) shows that the expected stable flow

distribution is $\dot{m}_1 \ll \dot{m}_2$ since it corresponds to a larger \dot{S}_{gen} than that associated with the unlikely flow distribution $\dot{m}_1 \gg \dot{m}_2$. Note that the stability criteria based on linear perturbation theory would not differentiate between the two cases and indicate that both cases $(\dot{m}_1 \gg \dot{m}_2 \text{ and } \dot{m}_1 \ll \dot{m}_2)$ are stable (with $\lambda < 0$).

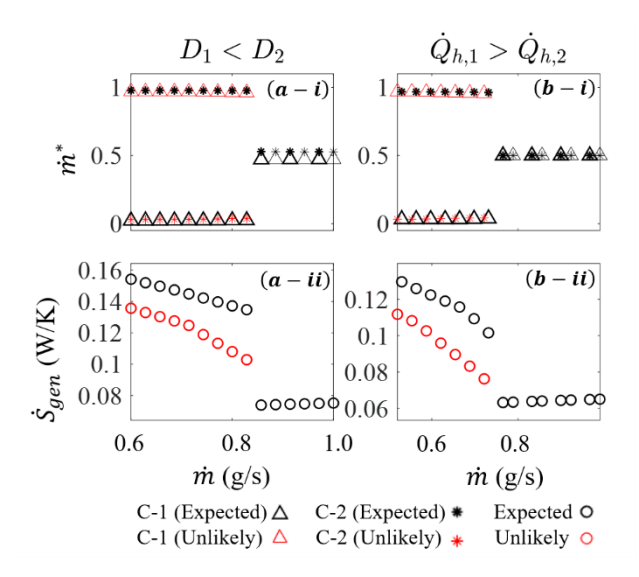


Figure 10. Comparison between expected (likely) and unlikely maldistributed flow states in a two parallel channel assembly for (a) $D_1 = 1.3$ mm, $D_2 = 1.4$ mm, and $\dot{Q}_{h,1} = \dot{Q}_{h,2} = 60$ W, and (b) $\dot{Q}_{h,1} = 60$ W, $\dot{Q}_{h,2} = 50$ W and $D_1 = D_2 = 1.4$ mm.

4.5.3 Parametric Study of Diameter and Heat Load

Figure 11 compares \dot{S}_{gen} for severely maldistributed flow solutions with $\dot{m}_1 \gg \dot{m}_2$ (blue) and $\dot{m}_1 \ll \dot{m}_2$ (red) as a function of $D_1^* = \frac{D_1}{D_1 + D_2}$ (left) and $\dot{Q}_{h,1}^* = \frac{\dot{Q}_{h,1}}{\dot{Q}_{h,1} + \dot{Q}_{h,2}}$ (right). In Figure 11(left), when $D_1^* < 0.5$, model predictions with $\dot{m}_2 \gg \dot{m}_1$ have a larger \dot{S}_{gen} compared to predictions with $\dot{m}_1 \gg \dot{m}_2$. Likewise, when $D_1^* > 0.5$, \dot{S}_{gen} is larger when $\dot{m}_1 \gg \dot{m}_2$ than $\dot{m}_1 \ll \dot{m}_2$. In Figure 11(right), \dot{S}_{gen} generally increases with an increase in $\dot{Q}_{h,1}^*$ due to higher irreversibility associated with a larger heat load. With $\dot{Q}_{h,1}^* < 0.5$, model predictions with $\dot{m}_1 \gg \dot{m}_2$ have a larger \dot{S}_{gen} than $\dot{m}_1 \ll \dot{m}_2$. With $\dot{Q}_{h,1}^* > 0.5$, a larger \dot{S}_{gen} is associated with $\dot{m}_1 \ll \dot{m}_2$ than $\dot{m}_1 \gg \dot{m}_2$. In

conclusion, the model-predicted flow distributions associated with a higher \dot{S}_{gen} are thermodynamically favored over other flow distributions satisfying the conservation laws.

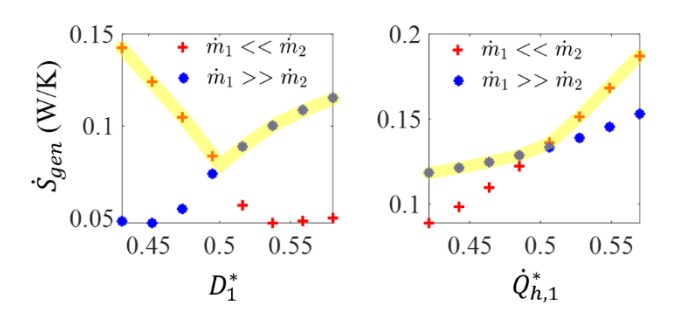


Figure 11. Comparison between \dot{S}_{gen} (at $\dot{m}=0.5$ g/s) corresponding to $\dot{m}_1\ll\dot{m}_2$ and $\dot{m}_1\gg\dot{m}_2$ maldistributed flow solutions for different values of D_1^* (at $\dot{Q}_{h,1}=\dot{Q}_{h,2}=60$ W and $D_2=1.4$ mm) and $\dot{Q}_{h,1}^*$ (at $D_1=D_2=1.4$ mm and $\dot{Q}_{h,2}=60$ W).

5 CONCLUSION

This study analyzes the relationship between two-phase flow distribution and entropy generation rate in a parallel channel assembly to address the challenge of a multiplicity of flow distribution solutions associated with the same conditions. The nonlinearity of the characteristic curves associated with two-phase flow in single channels indicates that stable theoretical solutions to flow distribution in a multi-channel network are often non-unique. In order to solve this challenge, previous studies applied linear stability analysis to determine the feasibility of a solution. However, this approach provides no underlying reason why a flow distribution is preferred over others, and it is limited in its applicability to distinguishing between stable and unstable flow distributions.

Therefore, we explore using an entropy analysis to predict the flow distribution in a two-parallel-channel network. In this study, entropy generation in parallel channel networks is divided into entropy generation within individual channels and entropy generation during the mixing of fluids at the shared headers of the parallel channel network. The entropy analysis in a single channel with

a constant heat load shows that hydraulic sources of irreversibility mainly drive entropy generation before the occurrence of CHF, while thermal sources of irreversibility become dominant after the occurrence of CHF. Also, entropy generation from mixing fluid at the shared exit is a function of the disparity in the thermal content of each channel fluid stream. We show that entropy generation in a severely maldistributed flow is greater than any unstable flow distribution under the same conditions. Therefore, during phase change and within given system constraints, severely maldistributed flow is thermodynamically favored over equally distributed flow or marginally nonuniform flow. Although severely maldistributed flow solutions are stable, these solutions are also non-unique. To distinguish between non-unique severely maldistributed flow solutions, we apply the trends observed from flow analyses in a single channel and in the common header of the parallel channel network to the differential equations describing the change in entropy generation rate. Through this, we show that for flow maldistribution under certain conditions, the resulting stable flow distribution corresponds to the highest rate of entropy generation, which is thermodynamically favored and will occur spontaneously. This conclusion is fundamental in understanding flow distribution in parallel channels and is applicable in optimizing the design of robust thermal systems against flow maldistribution.

6 SUPPLEMENTARY MATERIAL

The supplementary material describes the iterative process for solving the flow equations in the single and two-channel systems.

7 ACKNOWLEDGMENTS

S. Narayan acknowledges the financial support from the National Science Foundation's Division of Chemical, Bioengineering, Environmental, and Transport Systems in the Directorate for Engineering under Grant No. 1944323.

8 DATA AVAILABILITY STATEMENT

The data that support the findings of this study are available within the article.

9 CONFLICT OF INTEREST

The authors have no conflicts to disclose.

10 REFERENCES

- [1] J. C. Pacio and C. A. Dorao, "A study of the effect of flow maldistribution on heat transfer performance in evaporators," *Nuclear Engineering and Design*, vol. 240, no. 11, pp. 3868–3877, Nov. 2010, doi: 10.1016/j.nucengdes.2010.09.004.
- [2] T. Van Oevelen, J. A. Weibel, and S. V. Garimella, "Predicting two-phase flow distribution and stability in systems with many parallel heated channels," *International Journal of Heat and Mass Transfer*, vol. 107, pp. 557–571, 2017.
- [3] C. Guermonprez, S. Michelin, and C. N. Baroud, "Flow distribution in parallel microfluidic networks and its effect on concentration gradient," *Biomicrofluidics*, vol. 9, no. 5, Sep. 2015.
- [4] B. H. Lim, E. H. Majlan, W. R. W. Daud, M. I. Rosli, and T. Husaini, "Numerical analysis of flow distribution behavior in a proton exchange membrane fuel cell," *Heliyon*, vol. 4, p. 845, 2018.
- [5] T. Aka and S. Narayan, "Transient Behavior and Maldistribution of Two-Phase Flow in Parallel Channels *IEEE Transactions Components Packaging Manufacturing Technology*, vol. 12, no. 2, pp. 270–279, Feb. 2022.

- [6] T. Zhang, J. T. Wen, A. Julius, Y. Peles, and M. K. Jensen, "Stability analysis and maldistribution control of two-phase flow in parallel evaporating channels," *International Journal of Heat and Mass Transfer*, vol. 54, no. 25–26, pp. 5298–5305, Dec. 2011.
- [7] Y. Taitel and D. Barnea, "Transient solution for flow of evaporating fluid in parallel pipes using analysis based on flow patterns," *International Journal of Multiphase Flow*, vol. 37, no. 5, pp. 469–474, 2011.
- [8] U. Minzer, D. Barnea, and Y. Taitel, "Flow rate distribution in evaporating parallel pipes-modeling and experimental," *Chemical Engineering Science*, vol. 61, no. 22, pp. 7249–7259, 2006.
- [9] G. Patankar and T. R. Salamon, "Maldistribution of Two-Phase Flow in Parallel Channel Heat Sinks: Effects of Thermal Connection between Channels," *Proceedings of the 17th InterSociety Conference on Thermal and Thermomechanical Phenomena in Electronic Systems, ITherm 2018*, pp. 653–663, 2018, doi: 10.1109/ITHERM.2018.8419551.
- [10] Q. Jin, "Limit cycle analysis and maldistribution mitigation for multi-channel cooling system," *Applied Thermal Engineering*, vol. 204, Mar. 2022, doi: 10.1016/j.applthermaleng.2021.117982.
- [11] M. N. Hossain and K. Ghosh, "Entropy generation minimization for boiling flow inside evaporator tube with R32 and R410A refrigerants: a comparison of different two-phase flow models," *Journal of Thermal Science and Engineering Applications*, pp. 1–38, Feb. 2023.
- [12] O. S. Ezeora and O. Ezeora, "Purdue e-Pubs Entropy Generation Analysis and Optimum Tube Length of Two-Phase Flow Evaporator Tube Entropy Generation Analysis

- and Optimum Tube Length of Two-Phase Flow Evaporator Tube." [Online]. Available: http://docs.lib.purdue.edu/iracc/961
- [13] J. C. Ordóñez and A. Bejan, "Entropy generation minimization in parallel-plates counterflow heat exchangers,", "International Journal of Energy Research, vol. 24, no. 10, pp. 843–864, Aug. 2000.
- [14] L. S. Maganti and P. Dhar, "Consequences of flow configuration and nanofluid transport on entropy generation in parallel microchannel cooling systems," *International Journal of Heat and Mass Transfer*, vol. 109, pp. 555–563, 2017.
- [15] B. Sun, H. Chang, and Y. L. Zhou, "Flow regime recognition and dynamic characteristics analysis of air-water flow in horizontal channel under nonlinear oscillation based on multi-scale entropy," *Entropy*, vol. 21, no. 7, Jul. 2019.
- [16] P. Županović, D. Juretić, and S. Botrić, "Kirchhoff's loop law and the maximum entropy production principle," *Physical review. E, Statistical physics, plasmas, fluids, and related interdisciplinary topics*, vol. 70, no. 5, p. 5, 2004.
- [17] A. Miglani, J. A. Weibel, and S. V. Garimella, "An experimental investigation of the effect of thermal coupling between parallel microchannels undergoing boiling on the Ledinegg instability-induced flow maldistribution," *International Journal of Multiphase Flow*, vol. 139, Jun. 2021, doi: 10.1016/j.ijmultiphaseflow.2020.103536.
- [18] T. Aka and S. Narayan, "An entropic understanding of flow maldistribution in thermally isolated parallel channels," *International Journal of Heat and Mass Transfer*, vol. 227, p. 125564, Aug. 2024, doi: 10.1016/j.ijheatmasstransfer.2024.125564.

- [19] Q. Jin, J. T. Wen, and S. Narayanan, "Temperature synchronization across parallel microchannels during flow boiling," *International Journal of Thermal Sciences*, vol. 156, Oct. 2020, doi: 10.1016/j.ijthermalsci.2020.106476.
- [20] Q. Jin, J. T. Wen, and S. Narayanan, "Moving boundary model for dynamic control of multi-evaporator cooling systems facing variable heat loads," *International Journal of Refrigeration*, vol. 120, pp. 481–492, Dec. 2020, doi: 10.1016/j.ijrefrig.2020.09.014.
- [21] Q. Jin, J. T. Wen, and S. Narayanan, "The analysis and prediction of pressure drop oscillation in phase-change cooling systems," *International Journal of Heat and Mass Transfer*, vol. 165, Feb. 2021, doi: 10.1016/j.ijheatmasstransfer.2020.120621.
- [22] Q. Jin, J. T. Wen, and S. Narayanan, "Dynamic control of microchannel cooling system with unanticipated evaporator heat loads," *Applied Thermal Engineering*, vol. 183, Jan. 2021, doi: 10.1016/j.applthermaleng.2020.116225.
- [23] Q. Jin, J. T. Wen, and S. Narayan, "Effect of Oscillatory Heat Load on Pressure Drop Oscillation," *International Journal of Heat and Mass Transfer*, vol. 194, Sep. 2022, doi: 10.1016/j.ijheatmasstransfer.2022.123077.
- [24] V. Bellos, I. Nalbantis, and G. Tsakiris, "Friction Modeling of Flood Flow Simulations," *Journal of Hydraulic Engineering*, vol. 144, no. 12, Dec. 2018.
- [25] F. Incropera and D. DeWitt, *Fundamentals of Heat and Mass Transfer*, 6th ed. Hoboken, NJ: Wiley, 2007.
- [26] S. M. Kim and I. Mudawar, "Universal approach to predicting saturated flow boiling heat transfer in mini/micro-channels Part II. Two-phase heat transfer coefficient," *International Journal of Heat and Mass Transfer*, vol. 64, pp. 1239–1256, 2013.

- [27] J. C. Chen, F. T. Ozkaynak, and R. K. Sundaram, "Vapor heat transfer in post-CHF region including the effect of thermodynamic non-equilibrium," *Nuclear Engineering and Design*, vol. 51, no. 2, pp. 143–155, Jan. 1979.
- [28] Q. Jin, J. T. Wen, and S. Narayanan, "Analysis and Active Control of Pressure Drop Oscillation in Microchannel Vapor Compression Cycle," in 2018 17th IEEE Intersociety Conference on Thermal and Thermomechanical Phenomena in Electronic Systems (ITherm), IEEE, May 2018, pp. 842–849.
- [29] Toochukwu Aka (2023). Uncertainty_Prop (https://www.mathworks.com/matlabcentral/fileexchange/127853-uncertainty_prop),
 MATLAB Central File Exchange. Retrieved August 12, 2023.
- [30] M. Baikin, Y. Taitel, and D. Barnea, "Flow rate distribution in parallel heated pipes," *International Journal of Heat and Mass Transfer*, vol. 54, no. 19–20, pp. 4448–4457, 2011.